Effects of ceiling fans on airborne transmission in an air-conditioned space

Wenxin Li [a], Adrian Chong [a,*], Takamasa Hasama [b], Lei Xu [a], Bertrand Lasternas [a], Kwok Wai Tham [a], Khee Poh Lam [c]

[a] Department of Building, School of Design and Environment, National University of Singapore, Singapore
[b] Kajima Technical Research Institute Singapore, Singapore
[c] Department of Architecture, School of Design and Environment, National University of Singapore, Singapore

ARTICLE INFO

ABSTRACT

Indoor airborne transmission largely depends on air distribution and ventilation. This study experimentally and numerically investigates steady-state aerosol transmission characteristics in a full-size room using a dedicated outdoor air system coupled with ceiling fans. Tracer gas was used to simulate the exhaled droplet nuclei from the infector, and a breathing thermal manikin was employed as a seated exposed person. Effects of air supply rates, ceiling fan speeds, source positions, and breathing modes of the exposed person on the aerosol transmission were studied. The increase of air change per hour from 4.5 to 5.6 and 7.5 reduced the averaged concentrations at sampling points by 18% and 38%, respectively. The ceiling fans generated local air movement and mixed air within the space, and a higher operating speed contributed to a more uniform concentration distribution. With better dispersion of the aerosols, the ceiling fan operation reduced the concentrations at the exposed person's breathing zone by more than 20%. The ceiling fans show the potential to reduce the cross-infection risk in an air-conditioned space.

1. Introduction

The ongoing pandemic of coronavirus disease 2019 (COVID-19) has infected over 84.4 million people and caused 1.84 million deaths worldwide as of Jan 02, 2021 [1], and the numbers are increasing. Caused by the severe acute respiratory syndrome coronavirus 2 (SARS-CoV-2), the disease is transmitted through large droplets, fomites, and aerosols [2,3]. The SARS-CoV-2 virus could remain viable in aerosols throughout a 3-hour experiment [4]. The virus can be transmitted efficiently via the respiratory droplets and/or aerosols between ferrets from 3 to 7 days after exposure [5]. Most droplets and aerosols are dominated by short-range airborne transmission, especially during close contact (<2 m) exposure [6]. Compared to the large droplets, the small droplets diffuse faster, farther, and wider [7], being easier to suspend in the air. The probable aerosol transmission in poorly ventilated places has been supported by evidence from hospital wards [8], restaurants [9], and offices [10].

In indoor environments, airborne transmission by droplets and aerosols largely depends on the air distribution and ventilation; adequate and effective ventilation for mitigation should be ensured. This requires an increase in the amount of clean outdoor air supplied to indoor volumes [11], which can be achieved by increasing the ventilation rates (outdoor air change rate) and eliminate air-recirculation within the ventilation system [12]. However, an experimental study in the patient rooms suggested that the increasing ventilation rates failed to reduce aerosol concentrations proportionately. It could generate more particles suspending and migrating in pathways between the source and exhaust [13]. For a patient room with overhead mixing ventilation, the cross-infection risk still existed even at a high ventilation rate of up to 12 h^{-1}, which also brought draught discomfort in the occupied zone [14]. Thus, the ACH should not be used as the sole indicator of the system's ability to reduce exposure risk. The airflow pattern plays a vital role in influencing the dispersion of cough droplets and consequential exposure [15].

The airflow pattern is primarily determined by the ventilation configurations. Previous research has evaluated the influences of mixing ventilation [16], displacement ventilation [17], under-floor air distribution [18], downward ventilation [19], and stratum ventilation [20] on indoor airborne transmission. Many of them engaged in comparing the ventilation performances of different ventilation strategies; however, their conclusions strongly relied on the boundary condition setting of the test room [21]. For example, since the exhaled jet traveled a short

distance and then diluted quickly under the mixing ventilation, it performed better than the displacement ventilation in a tracer gas experiment [22], while worse in a numerical study with different room settings [23]. Generally, the well-mixing ventilation could efficiently remove the fine particles which strictly followed the airflow pattern. Simultaneously, the concentrations were also affected by the source position and its local airflow for the coarse particle transmission [24]. To improve the local ventilation at the occupants, advanced ventilation technologies including personalized ventilation [25] and ventilation fans [26,27] were supplemented to the basic ventilation configurations.

Recently, there has been increasing interest in using the dedicated outdoor air system coupled with ceiling fans (DOAS-CF) to achieve energy savings while maintaining occupant comfort. The DOAS-CF comprises a dedicated outdoor air system (DOAS) and ceiling fans (CF) in the occupied zones. This DOAS system supplies 100% outdoor air, conditioned by an appropriately sized cooling coil to the room. Air is exhausted via pressure-activated openings, and there is no recirculation. The DOAS-CF proposes to achieve energy savings by raising the cooling set-point (27–28 °C) of the cooling system, an effective energy-saving strategy in hot and humid climates [28]. Ceiling fans are then used to offset any discomfort caused by the warmer temperature with the elevated air movement. The combination of 27 °C and an air velocity of 0.94 m/s in DOAS-CF was experimentally proven to give the most satisfactory thermal comfort and air quality even compared with the 24 °C conventional air-conditioning system [28,29]. To maximize the many benefits of integrating ceiling fans with building systems, a ceiling fan design guide has also been developed [30]. However, the influence of ceiling fans on the airborne transmission is unknown, and the trade-offs between ventilation rate and ceiling fan speeds in DOAS-CF with regards to the transmission risk are not clear.

The COVID-19 pandemic ushers a "new normal" where the air-conditioning system operation should address airborne respiratory transmission in the post-pandemic era. Thus, this study aims to elucidate experimentally, and numerically the aerosol transmission behavior of ceiling fans integrated air-conditioning and mechanical ventilation (ACMV) systems. The objectives are:

- Investigate the effect of ceiling fans on aerosol transmission in an air-conditioning system with ceiling fans.
- Analyze the relationship between ceiling fan speed and ventilation rate on the airborne transmission.
- Evaluate the inhalation intake risks of the exposed person under different air-conditioning scenarios.

To do so, spatial contamination distributions were measured when a breathing thermal manikin (exposed person) seated 1.5 m opposite the tracer gas source (simulating an infector) inside a test room operating with DOAS-CF. The measurements of air velocity and concentration were used to validate a numerical model, subsequently providing detailed velocity, temperature, and concentration distributions. The effects of breathing modes of the exposed person, ceiling fan speeds, air supply rates, and source (infector) positions on velocity, temperature, concentration, and infection risks were investigated through a series of experiments and simulations. This study will provide a better understanding of the ceiling fans' effects on airborne transmission, and contribute to the future design of ceiling fans integrated ACMV systems.

2. Methods

2.1. Experiments

2.1.1. Experimental site

The experiments were conducted in a 9.9 m × 6.3 m × 3.65 m classroom in the School of Design and Environment 4 (SDE4) building at the National University of Singapore. A dedicated outside air system (DOAS) supplies conditioned air to the test room from four air diffusers

(0.35 m × 0.2 m) at the height of 3.06 m. The room air temperature is controlled at 27 ± 0.5 °C. During the experiments, indoor relative humidity was measured to vary between 70% and 85%. Supply air temperatures are between 17 and 19 °C. The air supply volume is controlled by the fan speed of the air handling unit (AHU), which varies from 30 Hz to 50 Hz. The DOAS creates positive pressure in the test room, and the indoor air exfiltrates through a transfer air device installed on the top of the door, which is the only outlet of this room.

Additionally, four ceiling fans (Big Ass Fans, Haiku 52) with a diameter of 1.32 m were installed at the height of 2.65 m in this room. Each ceiling fan has three airfoils and speeds in 7 phases (60 RPM - 182 RPM). To investigate the effects of ceiling fan speed on spatial concentration distribution, ceiling fan modes of 0 (off), 3 (100 RPM), and 5 (140 RPM) were selected and tested in this study, and their air velocities were measured to be 0.04, 1.10 and 1.92 m/s at the height of 1.1 m directly under the ceiling fan [28], respectively.

2.1.2. Experimental equipment

In this study, the tracer gas technique simulated the transmission of exhaled virus-laden droplet nuclei of 5–10 μm. Due to the scarcity in the environment, the common-used sulfur hexafluoride (SF_6) was selected as the tracer gas to release from an infected person, hereinafter referred to as the infector. A breathing thermal manikin was used to simulate the person exposed to the tracer gas, hereinafter referred to as the exposed person.

The breathing thermal manikin (P. T. Teknik Limited, Denmark) has the body shape and size of an average adult woman of 1.68 m in height. The manikin consists of 26 body segments that were heated and controlled individually to keep surface temperatures close to the skin temperature of a person in the state of thermal comfort [31]. In this experiment, the manikin was dressed in clothing corresponding to 0.5 clo (short-haired wig, short sleeve shirt, pants, underwear, socks, and shoes) to emulate a typical office worker in Singapore (0.44 clo) [32]. The manikin's heat power was approximately 65 W/m². The thermal manikin creates a bodily thermal plume and simulates realistic free convection flow around the human body. With a set of artificial lungs, the manikin simulates inhalation through the nose and exhalation through the mouth. The pulmonary ventilation rate was 6.0 L/min, and each breathing cycle consisted of 2.5 s inhalation, 2.5 s exhalation and a 1.0 s break. The exhaled air was heated to 34.7 °C, without being humidified. The nostrils are two 50.2 mm² circular openings, and the mouth is a 98.1 mm² semi-ellipsoidal opening. The two jets from the nostrils are angled 45° downwards from the horizontal plane and 30° from each other.

The SF_6 concentrations were sampled and measured through an INNOVA 1312 photo-acoustic multi-gas analyzer and an INNOVA 1309 multi-channel sampler with an accuracy of 0.001 ppm.

2.1.3. Experimental design

Fig. 1 shows the experimental setup inside the test room. The breathing thermal manikin is placed in a seated position on a chair with a desk in front. Directly opposite the manikin is a tracer gas tube fixed at 1.1 m (nose-to-ground height of a sitting manikin) above the ground. The distance between the source and the manikin is 1.5 m, a threshold distance to distinguish the short-/long-range airborne routes [33]. The distance from the manikin's abdomen to the table is 0.1 m.

1) Tracer gas decay test

Tracer gas decay tests were used to calculate the ACH of scenarios with ceiling fans at Mode 0 and 3 and AHU fan speeds at 30 (minimum), 32, 40, and 50 (maximum) Hz. 32 and 40 Hz were selected between the minimum and maximum speeds, which were commonly used in practice. At the beginning of the test, tracer gas was released and mixed for 30 s. The decayed concentration at the room center was recorded over 90 min for ACH calculation.
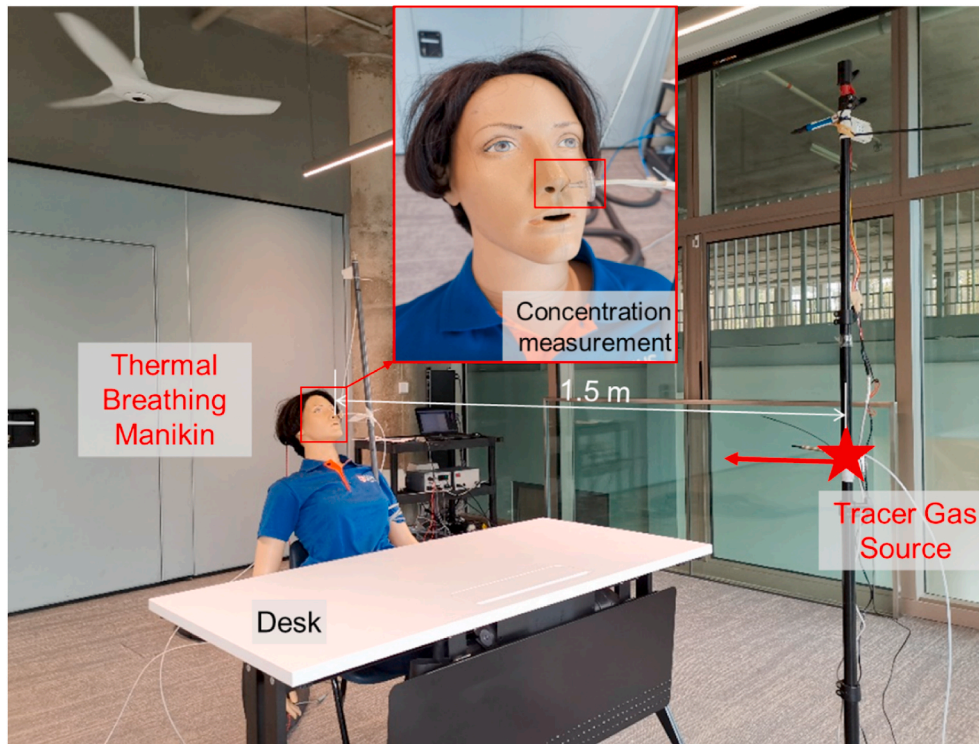
Fig. 1. Experimental setup: a thermal breathing manikin located 1.5 m opposite the tracer gas source. An aerosol sampling probe was positioned 5 mm below the tip of the manikin's nose to measure the SF_6 concentration at the breathing zone.

2) Tracer gas continuous injection test

Tracer gas was introduced via continuous injection to simulate the steady-state aerosol release and transmission. Tracer gas dosing started after indoor airflow distribution had reached steady-state conditions. Before starting each experiment, the initial SF_6 concentration was checked to ensure that the background concentrations were negligible (≤ 0.02 ppm). The tracer gas was released at a dosing rate of 0.04 L/min, calculated by BS ISO 16000–8:2007 [34]. The tracer gas release tube had a diameter of 0.008 m and was placed horizontally. The concentrations at six sampling points inside the test room were measured roughly every 5 min. The measurements during the steady-state period from 40 min to 110 min at each point were averaged for analysis.

As shown in Fig. 2, the continuous injection tests were conducted with the tracer gas source located in two locations: (1) directly under the ceiling fan (Location 1) and (2) at the room center (Location 2). A total of six sampling points measuring SF_6 concentration was placed inside the room for each location, and they include:

- Two sampling points close to the manikin's breathing zone located at 1.1 m (C1 in Location 1; C7 in Location 2) and 1.7 m (C2 in Location 1; C8 in Location 2) from the ground, corresponding to the nose height of a seated and a standing person, respectively. The sampling probe positioned 5 mm below the tip of the manikin's nose to measure the concentration at 1.1 m breathing zone (as indicated in the box in Fig. 1).
- Three sampling points surrounding the manikin in the room (C3, C4, C5 in Location 1; C9, C10, C11 in Location 2).
- One sampling point at the room outlet (C6 in Location 1; C12 in Location 2).

To investigate the effects of breathing modes, ceiling fan speeds, air supply rates and source positions on the airborne transmission, a total of 11 tests were designed and listed in Table 1. All ceiling fans operated at the same fan speed in each test.

2.2. Numerical simulations

2.2.1. CFD model

As shown in Fig. 3, a three-dimensional numerical model was built based on the test room. The air-conditioning ducts were not considered to reduce the computational cost. The air was supplied from the diffusers at the top of the room and exhausted through the outlet located on the sidewall. The supply air temperature was 19 °C, and its supply rate at the diffuser was measured to be 1.7, 2.2, and 2.8 m/s when AHU fan speeds operating at 32, 40, and 50 Hz, respectively.

The whole room domain, including the manikin and ceiling fans, were discretized using polyhedral mesh. The thermal manikin geometry was 3D scanned and then smoothed with the overall and critical features preserved. The manikin's clothes and wig were omitted due to their negligible effects on heat transfer and airflow. To accurately capture the near-wall gradients, manikin's surrounding mesh was refined with ten inflation layers to contain the viscous sub-layer (Fig. 3); the remaining less significant surfaces were applied with relative coarse mesh. The thermal manikin surface temperatures were measured to be 34.4 °C and 33.7 °C on average under scenarios of ceiling fan Modes 0 and 3, respectively. The radiative heat load was not considered in this study as it had a negligible impact on convective fluid dynamics. The multiple reference frame (MRF) model was used to calculate the rotating motion of the ceiling fans, and a rotating reference frame with a diameter of 1.5 m and a height of 0.6 m surrounded each ceiling fan. The surface temperature of interior walls was measured to be 27 °C, and the constant value was assumed for all the room ceiling, sidewalls, and floor in the simulations. The table and fans were assumed to be adiabatic. Since tracer gas was released slowly and effects of inertia or gravity on particles were negligible, the release point of tracer gas was represented by a small box ($50 \times 50 \times 50$ mm³) and simulated with the species transport model.

2.2.2. Governing equations

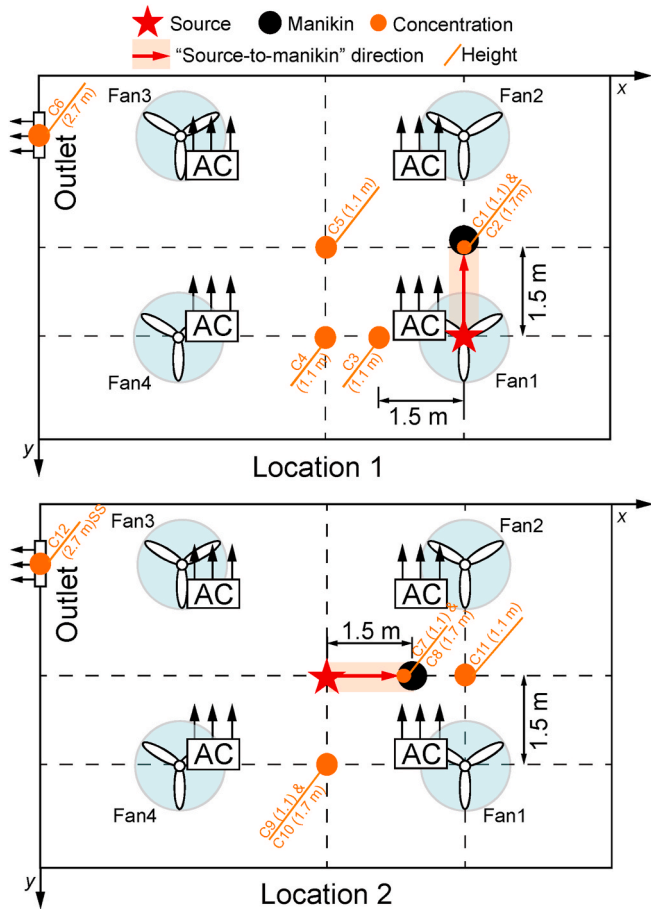In this study, the airflow field was solved using the incompressible

Fig. 2. SF$_6$ concentrations measured through sampling points C1~C6 at Location 1 (source under ceiling fan) and C7~C12 at Location 2 (source at room center).

Table 1
Cases tested in this study with AHU fan speeds of 0, 32, 40, and 50 Hz, ceiling fans operating at Mode 0, 3, and 5, at Locations 1 and 2.

Cases	Location	AHU fan speed (Hz)	Ceiling fan		Breathing
			Mode	Air velocity[a] (m/s)	
1	1	0	0	0.04	✓
2	1	32	0	0.04	✓
3	1	32	3	1.10	✓
4	1	32	5	1.92	✓
5	1	40	3	1.10	✓
6	1	50	3	1.10	✓
7	1	32	3	1.10	✗
8	2	0	0	0.04	✓
9	2	32	0	0.04	✓
10	2	32	3	1.10	✓
11	2	50	3	1.10	✓

[a] The air velocities were measured at 1.1 m height directly under the ceiling fan from Ref. [28].

Navier-Stokes equations incorporated with the Boussinesq approximation accounting for the thermal buoyancy flow induced by the occupant body heat. Realizable k-ε model was used to predict the distributions of airflow, temperature, and tracer gas. All governing equations were solved using the commercial CFD software ANSYS FLUENT 2020 R2 [35].

To solve the tracer gas dispersion, the species transport model with "passive scalar" was used:

$$\frac{\partial}{\partial t}(\rho Z) + \nabla \cdot (\rho Z u) = \nabla \cdot (\rho D \nabla Z) + S \quad (1)$$

where Z and u represent the mass fraction of tracer gas (kg per kg of air) and the airflow velocity vector, respectively; ρ is the air density; D is the contaminant's coefficient of diffusion with consideration of turbulence viscosity; S is the source term.

The rotating motion of ceiling fans was achieved with the multiple reference frame (MRF) model. It is a steady-state approximation in which individual cell zones can be assigned different rotational and/or translational speeds. This frozen rotor approach transfers the velocities entering the MRF region around the blades to a moving reference frame:

$$\overrightarrow{v}_{MRF} = \overrightarrow{v} - \overrightarrow{w} \times \overrightarrow{r} \quad (2)$$

where $\overrightarrow{v}$ is the velocity in the global (stationary) reference frame, $\overrightarrow{w}$ is the rotational vector and $\overrightarrow{r}$ is the position vector in the field of rotation.

The SIMPLE algorithm [35] was employed to couple the pressure and momentum equations. The second-order upwind scheme was used to discretize the convection and diffusion-convection terms in the governing equation.

The grid independency test was conducted before CFD simulations (Fig. 4). Once the grid element number exceeded 5.9 million, the airflow velocities at 0.1 m in front of the manikin (Fig. 4a) and directly under the ceiling fan (Fig. 4b) became stable. The maximum y+ value at the manikin surface was less than 3, indicating fine cells were obtained close to the manikin surface. Considering the computational efficiency and accuracy, the model with grid elements of 5,900,428 was used in this study.

2.3. Evaluation parameters

The ventilation rate of the whole test room was calculated by the air change rate (ACH). To reduce the unavoidable error from measurements, dimensionless contaminant concentration (ε) was used to evaluate the spatial concentration distribution inside the room. Moreover, intake fraction (IF) was used to assess the cross-infection risk at the breathing zone in this steady-state process.

ACH of the test room under different scenarios was calculated using experimental data from tracer gas decay tests. The concentration decay curve follows an exponential course when the gas mixes completely in the room. The air change per hour (ACH) is then calculated by Eq. (3).

$$ACH = \frac{\ln\left[\frac{C_1(t_1)}{C_2(t_2)}\right]}{t_2 - t_1} \quad (3)$$

where $C_1(t_1)$ and $C_2(t_2)$ are the tracer gas concentrations at the start and end of the test (ppm), respectively; t_1 and t_2 are the start and end time (s), respectively.

The dimensionless contaminant concentration (ε) expresses the ratio of the concentration in some sampling point (C_{point}) to the one at the outlet (C_{outlet}). It can reflect the overall uniformness and the contamination removal efficiency to some extent. This dimensionless concentration can be calculated as [36]:

$$\overline{\varepsilon(t)} = \frac{\overline{[C_{point}(t) - C_{supply}(t)]}}{\overline{[C_{outlet}(t) - C_{supply}(t)]}} \quad (4)$$

where C_{supply} is the tracer gas concentration (SF$_6$) in the supply air (ppm), which can be considered to be 0 in this study; The overhead bar indicates averaging during the period of t.

The concentration at the manikin's nose was used to calculate the inhalation IF of the exposed person (manikin). During a period of t under steady-state condition, IF is defined as the proportion of pollutant mass exhaled from the infector (source) that is then inhaled by the exposed
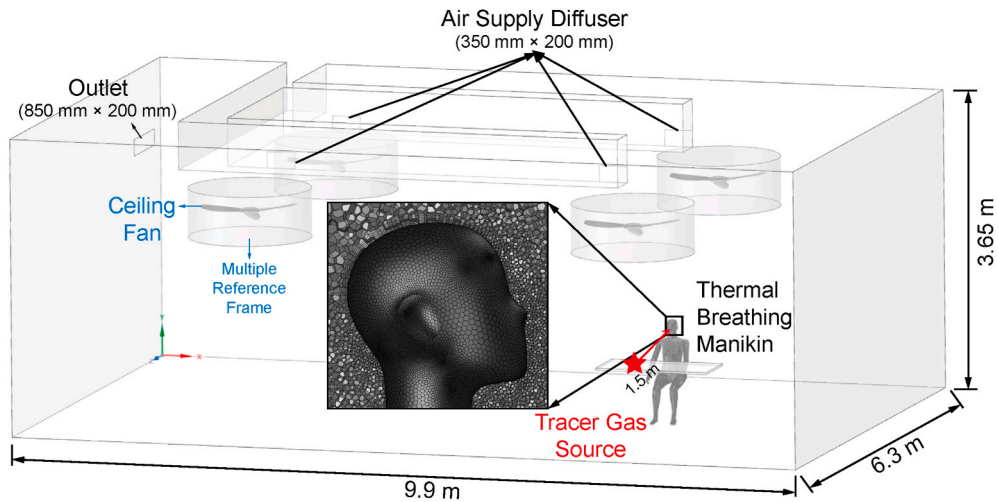
Fig. 3. Experimental site of Location 1 (source under ceiling fan); the enlarged figure shows the refined mesh around manikin's head used for simulation.

(a) Through the manikin (0.1 m in front) (b) Under the ceiling fan
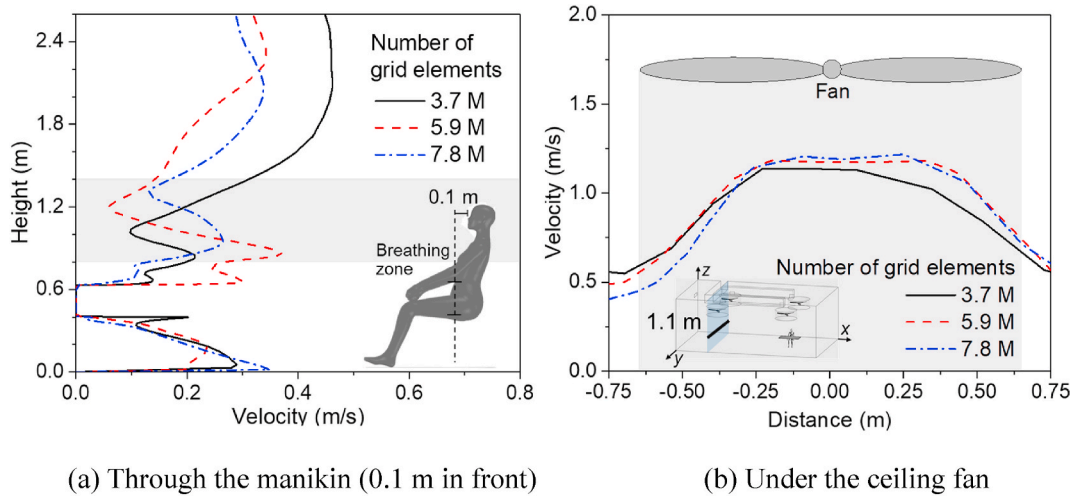
Fig. 4. Predicted velocity variations at cross-sections (a) through the manikin, 0.1 m in front of the nose ($x = 7.37$ m, $y = 3.25$ m) and (b) under the ceiling fan ($x = 2.53$ m, $z = 1.1$ m) for grid independency tests with grid elements numbers of 3.7, 5.9 and 7.8 million.

person (manikin), which can be written as:

$$IF = \frac{Q_B \cdot \int_0^t C_{in}(t)dt}{M_{released}} \quad (5)$$

where Q_B is constant breathing volume flow rate (m³/h); C_{in} is the inhaled concentration at manikin's nose (ppm); $M_{released}$ is the tracer gas amount at the source (μg/h).

Table 2
The linear relationship between ACH and AHU fan speeds (30–50 Hz) was measured by the tracer gas decay tests with ceiling fans operating at Mode 3.

AHU fan speed (Hz)	ACH
30	4.23
32	4.50
40	5.64
50	7.47

3. Results

3.1. System ACH

The ACH varied linearly with the AHU fan speed (Table 2). Under a forced mixing scenario with ceiling fans at Mode 3, the ACH increased from 4.23 to 7.37 when the AHU fan speed increased from 30 to 50 Hz.

3.2. Effect of breathing on airborne transmission

The effect of breathing modes was investigated by comparing the concentrations at 1.1 and 1.7 m close to the breathing and no breathing manikin (Fig. 5). When ceiling fans operated at Mode 3 and AHU fan speed at 32 Hz, concentrations increased averagely by 3.6% when the manikin changed from "breathing" to "no breathing". The hypothesis test (t-test) failed to reject the null hypothesis; thus, the breathing modes showed no significant difference in the concentrations (P = 0.29).

3.3. Effect of ceiling fans on airborne transmission

Considering the operation of ceiling fans, the numerical model was validated with the detailed measurements of air velocity and concentration at first. Then, the effects of ceiling fans on airborne transmission
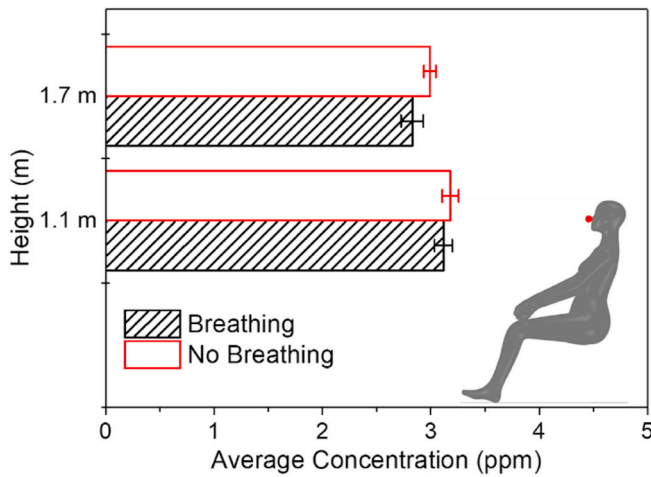
Fig. 5. Comparison of the SF_6 concentrations measured at heights of 1.1 m (manikin's nose) and 1.7 m close to the breathing and no breathing manikin.

were analyzed in detail at two locations: source (infector) under the ceiling fan (Location 1) and at the room center (Location 2).

3.3.1. CFD model validation

Firstly, the airflow distribution under a ceiling fan was compared with the measurements in the absence of any furniture. The measurements and simulations were conducted with AHU operating at a fan speed of 32 Hz and ceiling fans at Mode 3 at Location 1. The airspeeds at the heights of 0.6, 1.1, 1.7, and 2.2 m under the ceiling fan were measured by the omnidirectional hot-wire type anemometer (Kanomax, System 6244), which has an accuracy of ±0.1 m/s. The ceiling fans operated at Mode 3 during the tests. Since the turbulence caused by the sensor heat loss could easily affect the measurements, the simulated velocity magnitude (V) was corrected with turbulent kinetic energy (k)

[37] using the equation:

$$V = \sqrt{u^2 + v^2 + w^2 + 2k} \tag{6}$$

where u, v, and w are the velocities (m/s) in direction x, y, and z, respectively.

With no furniture underneath the ceiling fan, the predicted velocity under Fan 4 (fan center: $x = 2.53$ m, $y = 4.65$ m, $z = 2.6$ m) was used for comparison. As shown in Fig. 6, the airspeed predictions at all four heights matched the measurements well. The middle of the ceiling fan blade had high airspeeds due to the strong rotating airflow. Especially at heights of 1.7 and 2.2 m, the airspeed peaked at the blade while plunged at the ceiling fan center. The low velocity at the ceiling fan center was due to its short distance to the fixed center. For the breathing zone at 1.1 m, the mean absolute percentage error (MAPE) was 7.38%, and the root-mean-square error (RMSE) was 11.65%. The large discrepancy at 2.2 m attributed to the current turbulent model's limitation, which had little effect on the overall airflow analysis in this study. Error metrics for other heights are listed in Table 3.

Fig. 7 compares the measured and predicted concentration distributions at Locations 1 and 2 with AHU fan speed operating at 32 Hz. The predictions agreed well and shared a similar trend with the measurements of dimensionless concentration. The CFD model slightly under-predicted the concentrations when ceiling fans operating at Mode 0 while over-predicted at Mode 3. Their discrepancy is mainly attributed to the experimental uncertainty of the input mass flow rate. MAPE and RMSE for concentrations at Locations 1 and 3 when ceiling fans operating at Mode 0 and Mode 3 are listed in Table 3. The increase of ceiling fan speed from Mode 0 to Mode 3 provided more uniform concentration distributions. It decreased the concentration in the breathing zone at 1.1 m by 21% at Location 1 and 34% at Location 2.

3.3.2. Source (infector) under ceiling fan

At Location 1, where the source (infector) was under the ceiling fan, detailed analyses on the temperature, air velocity, and concentration
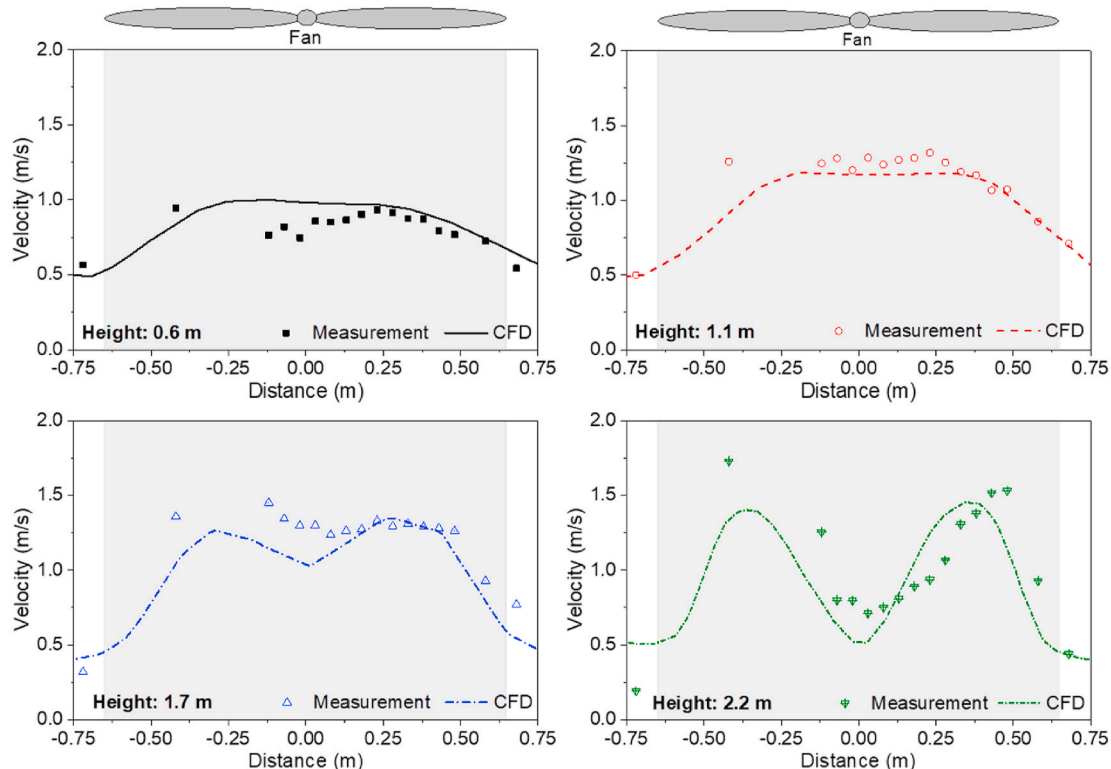

Fig. 6. Comparisons of simulated and measured velocities under the ceiling fan (when operating at Mode 3) at heights of 0.6, 1.1, 1.7, and 2.2 m.

Table 3
Error evaluations of measured and predicted velocities and concentrations.

Error metrics	Air velocity				Concentration			
	0.6 m	1.1 m	1.7 m	2.2 m	Location 1		Location 2	
					Fan Mode 0	Fan Mode 3	Fan Mode 0	Fan Mode 3
MAPE	12.64%	6.51%	12.15%	28.90%	11.90%	7.50%	7.48%	8.79%
RMSE	1.37%	10.94%	17.15%	25.89%	22.48%	15.37%	10.12%	16.69%

(a) Location 1

(b) Location 2

Fig. 7. Comparisons of predicted and measured dimensionless concentrations of six sampling points at (a) Location 1 (source under ceiling fan) and (b) Location 2 (source at room center) with ceiling fans operating at Mode 0 and Mode 3.

distributions were conducted. Fig. 8 compares the temperature and velocity contours with ceiling fans operating at Mode 0 and Mode 3 (AHU fan speed of 32 Hz). Significant thermal plume occurred when ceiling fans off (Mode 0). The upward thermal plume increased the temperature and air movements around the manikin. The strong upward thermal plume above manikin's head had an averagely 0.08 m/s higher air velocity than the unaffected area. When operating the ceiling fans at Mode 3, the strong downward airflow disturbed the thermal plume and changed the airflow distribution around the manikin. Specifically, ceiling fans directed the lateral airflow from diffusers towards the floor. They formed three circulation flows around the manikin: one at the back of the manikin and two on/under the table, respectively. They could mix the air in the space and give uniform temperature distributions. As shown in Fig. 8, since the left ceiling fan (Fan 1 center: $y = 4.05$ m) was overwhelmed with less cool supply air, the left half-space in this cross-section had a higher temperature when compared with the right half-space. The turbulent airflow environment caused by the operation of ceiling fans enhanced indoor ventilation. The volume-averaged age values were 439.9 s and 570.0 s for cases with ceiling fans at Mode 3 and Mode 0, respectively.

Fig. 9 shows the detailed streamlines formed by the supply air and ceiling fans operating at Mode 3. The fresh air was supplied from the diffuser inlets and then mixed with existing air. The ceiling fans accelerated the mixing and generated strong downward flows and circulations (Fig. 9a). Fig. 9b shows the streamlines in the room without the interaction of ceiling fans. The fresh air was injected almost laterally and then immediately absorbed by the ceiling fans, while the air from diffusers close to the walls reflected and flowed along the wall. Fig. 9c shows the streamlines seeded from ceiling fans (MRF surfaces), and it is clear that the ceiling fans generated downward flows directly underneath and circulations in each fan cell. Affected by the downward flow from the ceiling fan, the tracer gas flowed towards the floor and dispersed a short distance along the floor (Fig. 9d). However, for the scenario without ceiling fans, the air was circulated within the whole room (Fig. S1a), which carried the tracer gas to disperse around the room (Fig. S1b).

The strong air movements brought by ceiling fans also affected the tracer gas concentration distribution. Fig. 10 shows the simulated concentration contours at $x = 7.37$ m and $z = 1.1$ m with ceiling fans at Mode 0 and 3 at Location 1. The tracer gas formed a circle around the release point when ceiling fans operating at Mode 0, while a cone due to the downwards airflow at Mode 3. The static airflow without ceiling fan rotation (Mode 0) accumulated tracer gas around the release point and slightly moved towards the back wall (direction: y). Since the manikin was located at the leeward, the breathing zone had a relatively higher concentration. In contrast, the strong downward flow from ceiling fans extended the jet core area and formed a cone on the floor with ceiling fans at Mode 3. Similar to the temperature distribution in Fig. 8, the contaminant in the space covered by the left ceiling fan (Fan 1 center: $y = 4.05$ m) was well mixed. Meanwhile, the breathing zone had a low concentration because the table significantly blocked the upward flow towards the manikin's head.

Since ceiling fans' operation significantly decreased the concentrations at the breathing zone, the effect of ceiling fan speed on the concentration distribution was further analyzed with experimental data. As shown in Fig. 11, the increase of ceiling fan speed from Mode 0 to Mode 3 decreased the concentration in the breathing zone at 1.1 m by 21% and provided a more uniform concentration distribution. With a better mixing, a higher ceiling fan speed of Mode 5 gave a more uniform concentration distribution, with concentrations at each point steadying around 3.23 ppm.

3.3.3. Source (infector) at room center

For Location 2, where the source (infector) was located at the room center, the airflow and concentration distributions were analyzed. Even if Locations 1 and 2 had different airflow patterns, they gave a similar conclusion that the operation of ceiling fans decreased the concentrations at the breathing zone. With ceiling fans off, the concentration distribution at Location 2 was similar to that at Location 1, where a circle formed at the source point and contributed to a high concentration at the manikin's breathing zone. However, the downward flows from these four ceiling fans at Mode 3 impinged on the floor and generated local circulations and a strong upward flow at the room center (Fig. 12a). The velocity at the airflow confluence in the middle between the two ceiling fans (right under the ceiling fan in the cross-section $y = 3.15$ m in Fig. 12a) was around 0.2 m/s at 1.1 m height. For the source
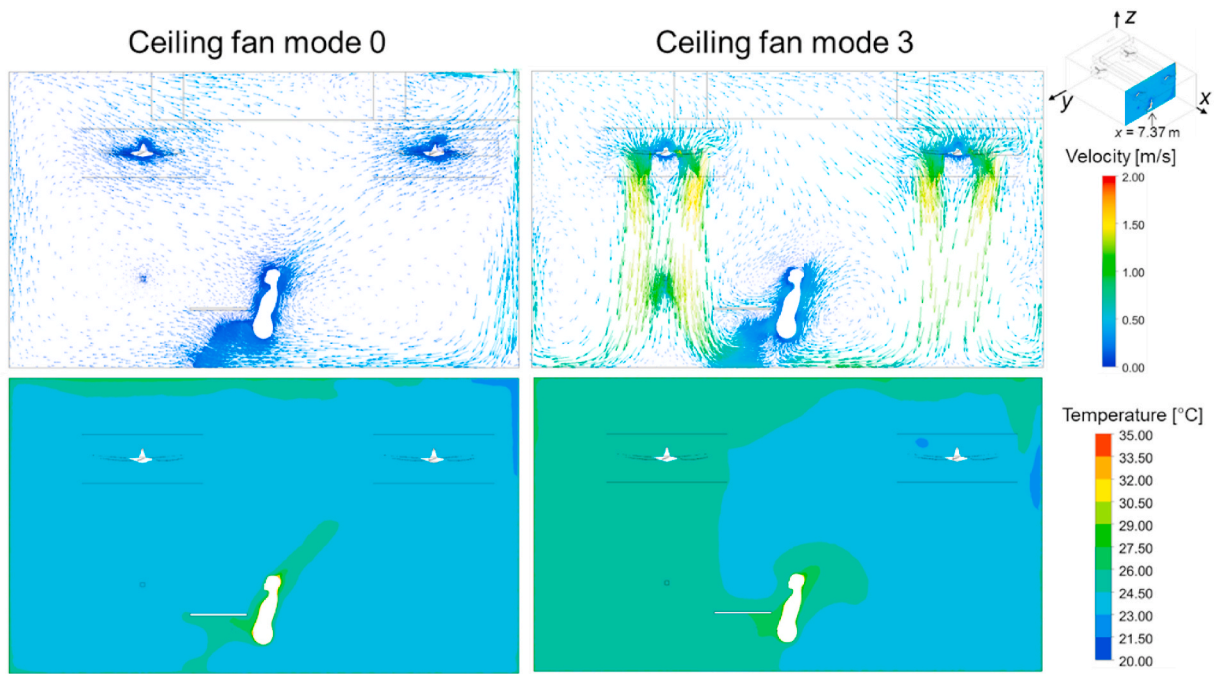
Fig. 8. Temperature and velocity contours at cross-section $x = 7.37$ m with ceiling fans operating at Mode 0 and 3 predicted by CFD.
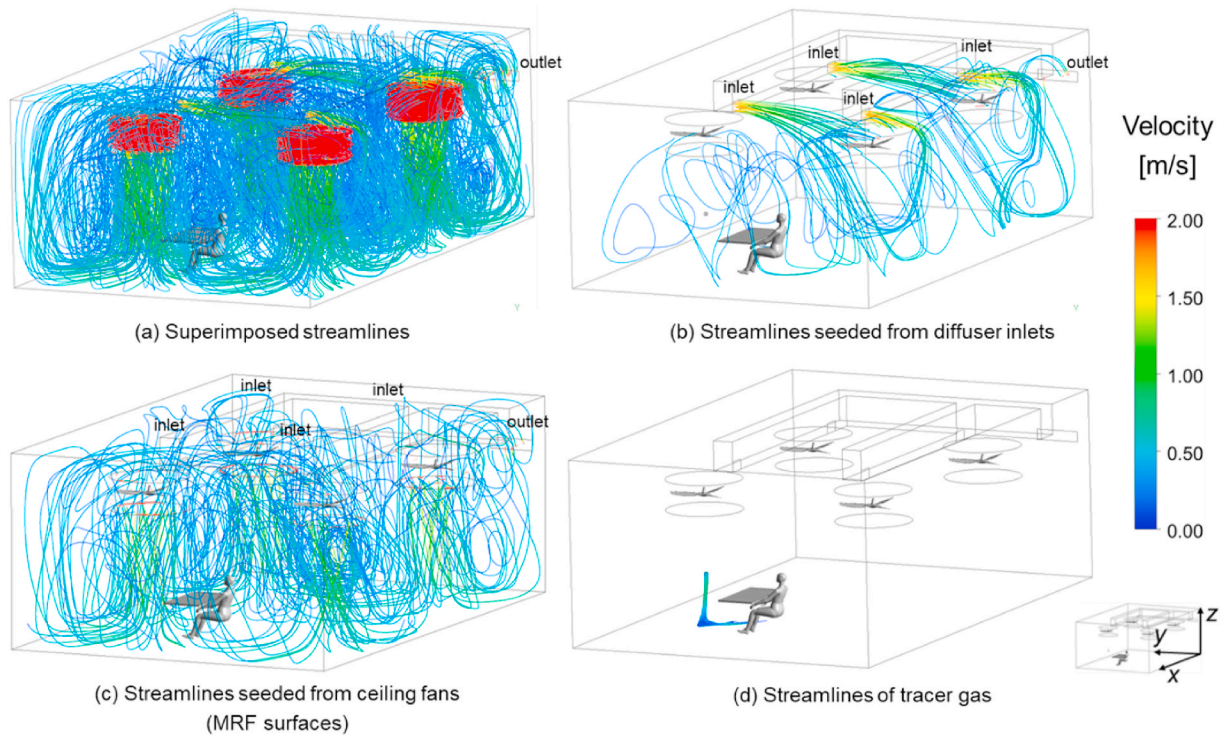

Fig. 9. (a) Superimposed streamlines and streamlines seeded from (b) the diffuser inlets, (c) ceiling fans, and (d) tracer gas at the scenario with ceiling fans at Mode 3 predicted by CFD.

position at room center, the airflow confluence of circulations was actually formed by four ceiling fans, and its velocity was up to 0.55 m/s. This air velocity was lower than the one measured right under the ceiling fan but strong enough to affect the surrounding air distribution. Thus, the upward air movement brought tracer gas towards the ceiling, resulting in a low breathing zone concentration (Fig. 12b). The concentration contour at $z = 1.1$ m clearly showed that ceiling fans' operation effectively impeded tracer gas dispersion in the breathing zone.

Similar interactions of airflow from ceiling fans and diffusers could be found in the streamlines in Fig. S2. However, the strong airflow could carry the tracer gas to disperse around the whole room (Fig. S2d).

3.4. Interactions between ventilation rate and ceiling fans

Based on the ceiling fan effect analysis, the interaction between ceiling fans and ventilation rate was further studied by comparing the
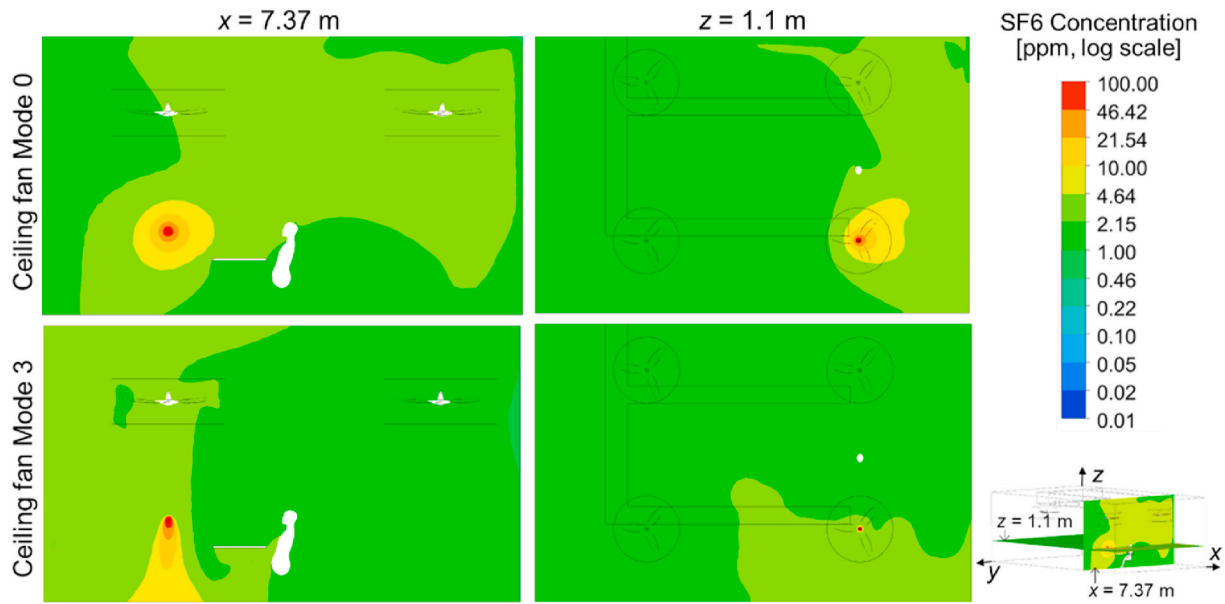
Fig. 10. Concentration contours at $x = 7.37$ m and $z = 1.1$ m with ceiling fans operating at Mode 0 and 3 at Location 1 (source under ceiling fan) predicted by CFD.
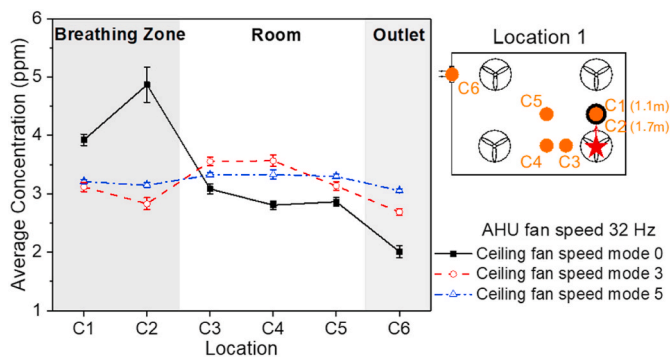

Fig. 11. Measured SF_6 concentration distributions at six sampling points with AHU fan speed at 32 Hz and ceiling fans operating at Mode 0, 3, and 5.

concentrations measured at six sampling points. When ceiling fans operating at Mode 3 at Location 1, the increase of AHU fan speeds significantly reduced the sampled locations average concentrations by 17.7% and 37.5% if the AHU fan speeds increased from 32 Hz (ACH = 4.50) to 40 Hz (ACH = 5.64) and 50 Hz (ACH = 7.47), respectively (Fig. 13). For these measured concentrations, a 26% increase in ACH reduced the average concentration by 18%, while a 66% increase in ACH contributed to a 38% reduction. The disproportionate reduction may attributed to aerosol dispersion throughout the room, notably from the breathing zone to the upper portion. Their concentrations shared similar distributions for these points, where the breathing zone had a relatively low concentration. It indicated that the ventilation rate determined the concentrations, and the detailed concentration distributions were dominated by the local airflow field affected by ceiling fans.

However, different ventilation rates gave different concentration distributions in Location 2 (source at room center). Operating at ceiling fan Mode 3, the increase of AHU fan speed from 32 Hz to 50 Hz decreased the sampled locations average concentration by 36% and the concentration at the outlet by 49.3% (1.42 ppm) (Fig. 14). With more air supplied (AHU fan speed at 50 Hz), the concentrations distributed uniformly within the space while much higher than the outlet value. The high dimensionless concentration in the room indicated that the tracer gas was not efficiently removed, even with a high ACH of 7.47. For this circumstance where the source was located at room center (Location 2)

and all sampling points at the confluence of airflows at the middle between two ceiling fans, the airflow was not strong enough to drive the tracer gas towards the outlet.

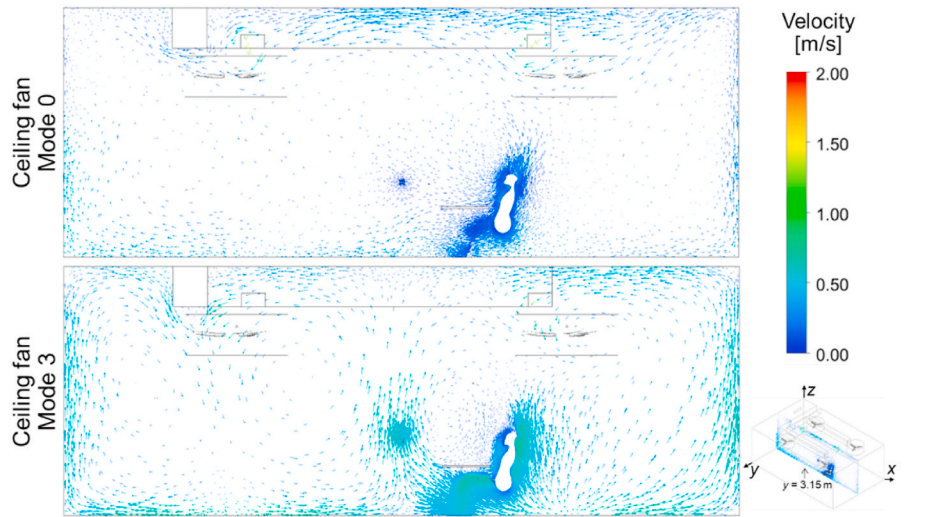### 3.5. Risk assessment at manikin breathing zone

Special attention has been paid to the cross-infection risks under different air-conditioning scenarios. For this relative comparison analysis, the inhalation intake fraction (IF) was calculated with the tracer gas concentrations measured at the manikin's nose (points C1 in Location 1 and C7 in Location 2). As shown in Fig. 15, the worst scenario without supply air and ceiling fans had an IF of 0.09, and most of the other air-conditioned scenarios had IF values less than 0.05. With the same supply air amount (AHU fan speed of 32 Hz), the increase of ceiling fan speeds from Mode 0 to Mode 3 decreased the IF values by 21.1% at Location 1 and by 24.3% at Location 2. For cases with ceiling fans at Mode 3 at both Locations 1 and 2, a 1 Hz AHU fan speed increase roughly resulted in a 2% decrease in IF value. Without the strong downward flow in Location 1, Location 2 had a slightly higher IF. The difference between these two source locations narrowed when ceiling fans were turned on.
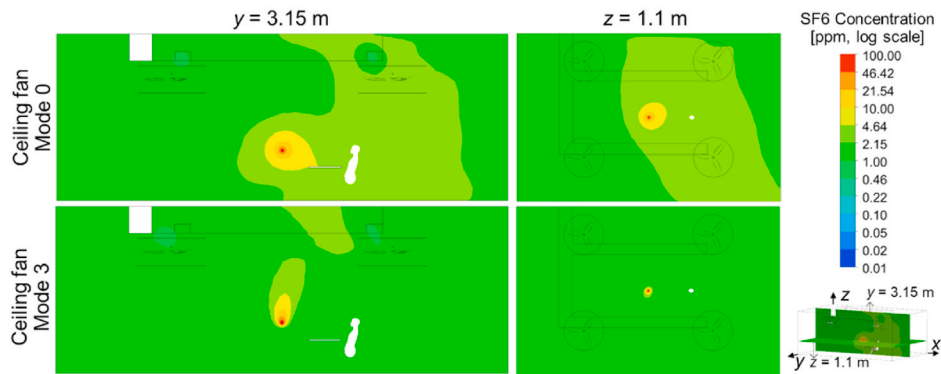
4. Discussion

In summary, ceiling fans can affect indoor aerosol transmission by:

1) Direct flow downwards for the zone underneath, and direct flow upwards when two local circulations meet at the middle of two ceiling fans. The infectious concentration distribution pattern strongly relates to the source position, which is subsequently affected by the specific airflow field generated by ceiling fans.
2) Mix air and average concentration within a space. If multiple ceiling fans are installed, space will be subdivided into multiple "fan cells", each of which behaves like a small space with a single fan.

Previous works observed that the ventilation fan could provide a well-mixed condition and uniform concentration distribution in the occupant vicinity [38]. The concept of "fan cells" was previously adopted in "*Ceiling Fan Design Guide*" [30], which referred to the subdivided space in the design stage. First, the overall layout was subdivided into multiple equal roughly square "fan cells", and then each cell was centered with a ceiling fan. In this study, we observed that the

(a) Velocity (y = 3.15 m)

(b) Concentration (y = 3.15 m and z = 1.1 m)

Fig. 12. Distribution contours of (a) velocity (y = 3.15 m) and (b) concentration (y = 3.15 m and z = 1.1 m) with ceiling fans operating at Mode 0 and 3 at Location 2 (source at room center) predicted by CFD.
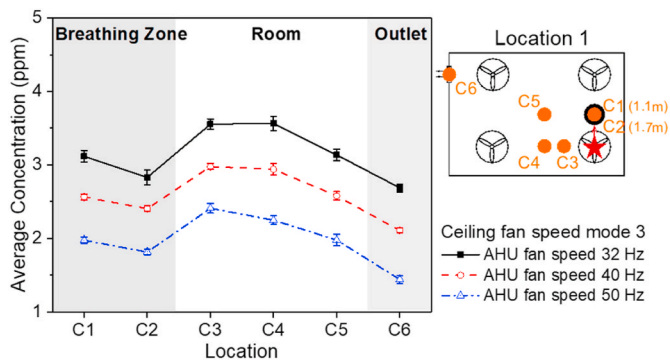

Fig. 13. Measured SF_6 concentration distributions at six sampling points with ceiling fans operating at Mode 3 and AHU fan speeds at 32, 40, and 50 Hz at Location 1 (source under ceiling fan).
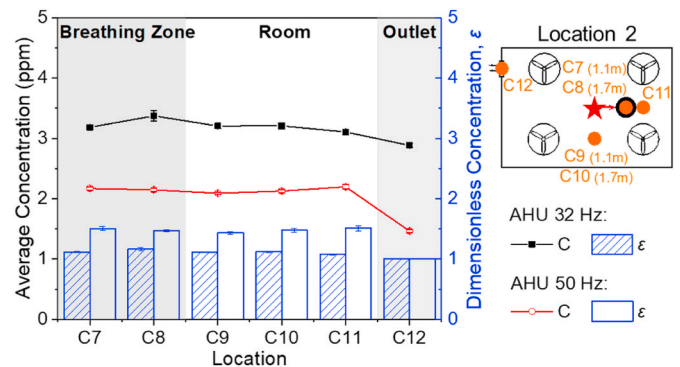

Fig. 14. Comparisons of concentration and dimensionless concentration (ε) of points in Location 2 (source at room center) with ceiling fans at mode 3, AHU fan speeds of 32 Hz and 50 Hz by measurement.

mixing was actually limited to each "fan cell" if multiple ceiling fans operated simultaneously. The "fan cell" was formed with an "air curtain", the confluence of airflows at the middle between two ceiling fans. Generally, the influence of local flow outweighs that of mixing on airflow and concentration distributions if the source is located at specific

positions, e.g., directly under the ceiling fan (Location 1) and at the "air curtain" between ceiling fans (Location 2) in this study. The upward-/downward flow could be advantageous since it reduced the direct exposure towards the breathing zone. The effects of direct flow and mixing brought by ceiling fans are coupled on airborne transmission,
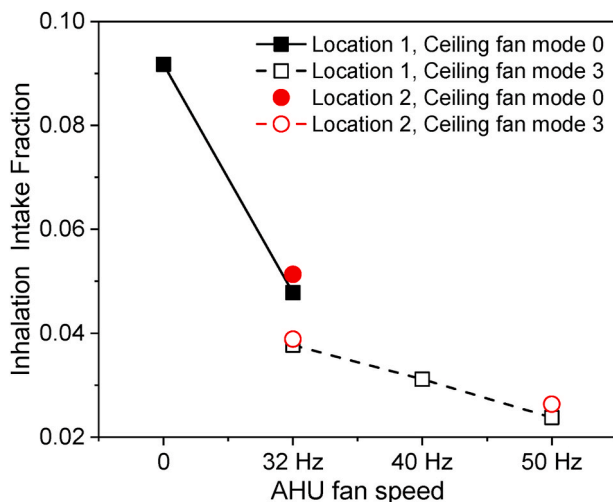
Fig. 15. Comparisons of inhalation intake fraction (IF) for each scenario based on measurements.

where the strong air movements will contribute to a well-mixed space.

Moreover, physical partitions, including people and tables, would affect the mixing. For example, the table performed differently in scenarios with ceiling fans on/off at Location 1 (Fig. 10). Since the source was located at the same height as the manikin's breathing zone, the table blocked the contamination dispersion when ceiling fans were not operating (turned off), which enabled a more significant movement of released tracer gas (simulating infectious droplets) towards the breathing zone. However, when running at Mode 3, the table beneficially impeded the upwards flow deflected from the floor and transported by the thermal plume, further reducing the concentrations at the breathing zone. It indicates that the physical partitions (e.g., tables) should be appropriately considered in the airflow field design.

The relationship between ceiling fan speed and ventilation rate on aerosol transmissions was investigated at two source positions in this study. The concentrations at sampling points at Location 1 (source under ceiling fan) reduced smoothly with the increase of AHU fan speeds (Fig. 13), while the non-uniform concentration distributions in Location 2 (source at room center) suggesting that tracer gas were not removed efficiently with ceiling fan operating at Mode 3 and AHU fan speed at 50 Hz (Fig. 14). The air velocity at the source position at Location 2 (0.55 m/s) was around half of that at Location 1 (1.10 m/s). The weak air movements at Location 2 limited the ventilation brought by the large volume of the supply air. It is estimated that a higher ACH of more than 7.47 (50 Hz) could not achieve a similar concentration reduction; thus, the increasing ACH could not guarantee good air quality in locations without sufficient ventilation. The observation is consistent with the conclusion that the local airflow pattern also plays an important role in the airborne transmission in addition to the ACH [15]. Since the approach of dilution ventilation (e.g., increasing ACH) has been recommended for controlling airborne diseases, its efficiency can be enhanced by optimized air distribution (e.g., application of ceiling fans or higher ceiling fan speeds).

This study focuses on the steady-state aerosol transmission with experiments conducted with tracer gas. However, there are some limitations of this study: 1) this study cannot represent the transient aerosol transmission; 2) the tracer gas technique used in this study cannot consider complicated dynamic processes, such as evaporation, condensation, coagulation, resuspension, and phase change; 3) this study provides a preliminary study for the fan cells, while further studies need to be conducted to understand better the fan cells and design of ceiling fan layouts.

5. Conclusion

Characteristics of the steady-state airborne transmission were investigated experimentally and numerically in this study. The effects of breathing mode, ceiling fan, and air supply on the airborne transmission were analyzed through the airflow, temperature, and concentration distributions. Moreover, cross-infection risks of different air distributions were evaluated. The conclusions arising from this study are summarized as follows:

(1) The airflow in the supply air only scenario (fans not operating) was affected mainly by the thermal plume, which contributed to a higher concentration at 1.7 m height in the breathing zone. In contrast, the fan operation scenario dispersed aerosols better, resulting in a more uniform concentration distribution, and a 20% lower concentration at the breathing zone. The increase of ceiling fan speeds contributed to a more uniform concentration distribution.
(2) Ceiling fans direct airflows in the local air distributions and mix air within the individual "fan cell" space (if multiple ceiling fans are applied). Thus, different concentration distributions will be obtained if the source position changes.
(3) The test room using the DOAS-CF system had high ACHs varying from 4.2 to 7.5 and a low inhalation intake fraction less than 0.05. The increase of ACH can significantly decrease the average concentration, and ceiling fans disperse aerosols from the breathing zone to the upper portion, contributing to further reducing the inhalation fraction.
(4) The breathing mode had a minor effect on the breathing zone's contamination distribution, which had an averaged discrepancy of 3.6% at a well-ventilated location with ceiling fans turned on.

Declaration of competing interest

The authors declare that they have no known competing financial interests or personal relationships that could have appeared to influence the work reported in this paper.

Appendix A. Supplementary data

Supplementary data to this article can be found online at https://doi.org/10.1016/j.buildenv.2021.107887.

References

[1] Worldometer's COVID-19 data, Retrieved 02 Jan, 2021, 04:09 GMT from, https://www.worldometers.info/coronavirus/?utm_campaign=homeAdvegas1?.
[2] L. Morawska, J. Cao, Airborne transmission of SARS-CoV-2: the world should face the reality, Environ. Int. 139 (2020), 105730.
[3] D. Lewis, Is the coronavirus airborne? Experts can't agree, Nature 580 (7802) (2020) 175.
[4] N. van Doremalen, T. Bushmaker, D.H. Morris, M.G. Holbrook, A. Gamble, B. N. Williamson, A. Tamin, J.L. Harcourt, N.J. Thornburg, S.I. Gerber, Aerosol and surface stability of SARS-CoV-2 as compared with SARS-CoV-1, N. Engl. J. Med. 382 (16) (2020) 1564–1567.
[5] M. Richard, A. Kok, D. de Meulder, T.M. Bestebroer, M.M. Lamers, N.M. Okba, M. F. van Vlissingen, B. Rockx, B.L. Haagmans, M.P. Koopmans, SARS-CoV-2 is transmitted via contact and via the air between ferrets, Nat. Commun. 11 (1) (2020) 1–6.
[6] W. Chen, N. Zhang, J. Wei, H.-L. Yen, Y. Li, Short-range airborne route dominates exposure of respiratory infection during close contact, Build. Environ. 176 (2020), 106859.

[7] X. Yang, C. Ou, H. Yang, L. Liu, T. Song, M. Kang, H. Lin, J. Hang, Transmission of pathogen-laden expiratory droplets in a coach bus, J. Hazard Mater. 397 (2020).

[8] K. Nissen, J. Krambrich, D. Akaberi, T. Hoffman, J. Ling, Å. Lundkvist, E. Salaneck, Long-distance Airborne Dispersal of SARS-CoV-2 in COVID-19 Wards, 2020.

[9] Y. Li, H. Qian, J. Hang, X. Chen, P. Cheng, L. Hong, S. Wang, et al., Probable airborne transmission of SARS-CoV-2 in a poorly ventilated restaurant, Build. Environ. 196 (2021) 107788.

[10] S.Y. Park, Y.-M. Kim, S. Yi, S. Lee, B.-J. Na, C.B. Kim, J.-i. Kim, H.S. Kim, Y.B. Kim, Y. Park, I.S. Huh, H.K. Kim, H.J. Yoon, H. Jang, K. Kim, Y. Chang, I. Kim, H. Lee, J. Gwack, S.S. Kim, M. Kim, S. Kweon, Y.J. Choe, O. Park, Y.J. Park, E.K. Jeong, Coronavirus disease outbreak in call center, South Korea, Emerging Infectious Disease journal 26 (8) (2020) 1666.

[11] ASHRAE, ASHRAE Position Document on Airborne Infectious Diseases, 2020.

[12] L. Morawska, J.W. Tang, W. Bahnfleth, P.M. Bluyssen, A. Boerstra, G. Buonanno, J. Cao, S. Dancer, A. Floto, F. Franchimon, C. Haworth, J. Hogeling, C. Isaxon, J. L. Jimenez, J. Kurnitski, Y. Li, M. Loomans, G. Marks, L.C. Marr, L. Mazzarella, A. K. Melikov, S. Miller, D.K. Milton, W. Nazaroff, P.V. Nielsen, C. Noakes, J. Peccia, X. Querol, C. Sekhar, O. Seppänen, S.I. Tanabe, R. Tellier, K.W. Tham, P. Wargocki, A. Wierzbicka, M. Yao, How can airborne transmission of COVID-19 indoors be minimised? Environ. Int. 142 (2020).

[13] E.S. Mousavi, K.R. Grosskopf, Ventilation rates and airflow pathways in patient rooms: a case study of bioaerosol containment and removal, Ann. Occup. Hyg. 59 (9) (2014) 1190–1199.

[14] Z.D. Bolashikov, A.K. Melikov, W. Kierat, Z. Popiołek, M. Brand, Exposure of health care workers and occupants to coughed airborne pathogens in a double-bed hospital patient room with overhead mixing ventilation, HVAC R Res. 18 (4) (2012) 602–615.

[15] J. Pantelic, K.W. Tham, Adequacy of air change rate as the sole indicator of an air distribution system's effectiveness to mitigate airborne infectious disease transmission caused by a cough release in the room with overhead mixing ventilation: a case study, HVAC R Res. 19 (8) (2013) 947–961.

[16] F.A. Berlanga, I. Olmedo, M.R. de Adana, J.M. Villafruela, J.F.S. José, F. Castro, Experimental assessment of different mixing air ventilation systems on ventilation performance and exposure to exhaled contaminants in hospital rooms, Energy Build. 177 (2018) 207–219.

[17] Y. Yin, W. Xu, J.K. Gupta, A. Guity, P. Marmion, A. Manning, B. Gulick, X. Zhang, Q. Chen, Experimental study on displacement and mixing ventilation systems for a patient ward, HVAC R Res. 15 (6) (2009) 1175–1191.

[18] N. Gao, J. Niu, L. Morawska, Distribution of Respiratory Droplets in Enclosed Environments under Different Air Distribution Methods, Building Simulation, Springer, 2008, pp. 326–335.

[19] P.V. Nielsen, Y. Li, M. Buus, F.V. Winther, Risk of cross-infection in a hospital ward with downward ventilation, Build. Environ. 45 (9) (2010) 2008–2014.

[20] Y. Lu, M. Oladokun, Z. Lin, Reducing the exposure risk in hospital wards by applying stratum ventilation system, Build. Environ. 183 (2020).

[21] Z. Ai, A.K. Melikov, Airborne spread of expiratory droplet nuclei between the occupants of indoor environments: a review, Indoor Air 28 (4) (2018) 500–524.

[22] H. Qian, Y. Li, P. Nielsen, C. Hyldgaard, T. Wong, A. Chwang, Dispersion of exhaled droplet nuclei in a two-bed hospital ward with three different ventilation systems, Indoor Air 16 (111–128) (2006). Indoor Air (2006).

[23] X. Li, J. Niu, N. Gao, Spatial distribution of human respiratory droplet residuals and exposure risk for the co-occupant under different ventilation methods, HVAC R Res. 17 (4) (2011) 432–445.

[24] D. Rim, A. Novoselac, Ventilation effectiveness as an indicator of occupant exposure to particles from indoor sources, Build. Environ. 45 (5) (2010) 1214–1224.

[25] J. Pantelic, G.N. Sze-To, K.W. Tham, C.Y. Chao, Y.C.M. Khoo, Personalized ventilation as a control measure for airborne transmissible disease spread, J. R. Soc. Interface 6 (suppl_6) (2009) S715–S726.

[26] K.W. Tham, J. Pantelic, Performance evaluation of the coupling of a desktop personalized ventilation air terminal device and desk mounted fans, Build. Environ. 45 (9) (2010) 1941–1950.

[27] L. Wong, W. Chan, K. Mui, A. Lai, An experimental and numerical study on deposition of bioaerosols in a scaled chamber, Aerosol. Sci. Technol. 44 (2) (2010) 117–128.

[28] K. Mihara, C. Sekhar, Y. Takemasa, B. Lasternas, K.W. Tham, Thermal comfort and energy performance of a dedicated outdoor air system with ceiling fans in hot and humid climate, Energy Build. 203 (2019), 109448.

[29] K. Mihara, B. Lasternas, Y. Takemasa, K.W. Tham, C. Sekhar, Indoor environment evaluation of a Dedicated Outdoor Air System with ceiling fans in the tropics – a thermal manikin study, Build. Environ. 143 (2018) 605–617.

[30] P. Raftery, D. Douglass-Jaimes, Ceiling Fan Design Guide, 2020.

[31] BYTELINE, Manikin manual, 2018 version 3.x, https://www.manikin.dk/download/manual.pdf.

[32] R.J. de Dear, K.G. Leow, S.C. Foo, Thermal comfort in the humid tropics: field experiments in air conditioned and naturally ventilated buildings in Singapore, Int. J. Biometeorol. 34 (4) (1991) 259–265.

[33] L. Liu, Y. Li, P.V. Nielsen, J. Wei, R.L. Jensen, Short-range airborne transmission of expiratory droplets between two people, Indoor Air 27 (2) (2017) 452–462.

[34] I. BS, ISO 16000-8: 2007 Determination of Local Mean Ages of Air in Buildings for Characterizing Ventilation Conditions, BSI, London, 2007.

[35] I. ANSYS, ANSYS Fluent Theory Guide, 2020. USA.

[36] Z. Ai, K. Hashimoto, A.K. Melikov, Airborne transmission between room occupants during short-term events: measurement and evaluation, Indoor Air 29 (4) (2019) 563–576.

[37] A.I.o. Japan, AIJ Benchmarks for Validation of CFD Simulations Applied to Pedestrian Wind Environment Around Buildings, 2016.

[38] D. Rim, A. Novoselac, Transport of particulate and gaseous pollutants in the vicinity of a human body, Build. Environ. 44 (9) (2009) 1840–1849.